Revisiting Intersystem Crossing Mechanisms in Chromophore Dimers through the lens of Excitonic Coupling: A Case Study of Naphthalimide

Monika G. Mutovska,[a] Darío Puchán Sánchez,[b] Arthur H. G. David,[b] Clément Cabanetos,[b] Tangui Le Bahers,[c,d] Yulian Zagranyarski,*[a] Cyrille Monnereau,*[c] and Josene M. Toldo[e*]*

[a] *Faculty of Chemistry and Pharmacy, Sofia University "St. Kliment Ohridski", 1 J. Baurchier blvd., 1164, Sofia, Bulgaria*
[b] *Univ Angers, CNRS, MOLTECH-ANJOU, SFR MATRIX, F-49000 Angers, France*
[c] *ENS de Lyon, CNRS, Laboratoire de Chimie UMR 5182, F-69342 Lyon, France*
[d] *Institut Universitaire de France, 5 rue Descartes 75005 Paris, France*
[e] *Université Lyon 1, ENS de Lyon, CNRS, Laboratoire de Chimie UMR 5182, Lyon, France*

Table of Contents

Experimental Section

S1. Materials and methods

Synthesis

Commercially available reagents and solvents of analytical grade (Merck, Germany and Fischer Scientific, UK) were used without further purification unless otherwise stated. *N*-(octyl)-4-bromo-1,8-naphthalimide (**1a**)[1], *N*-(2-ethylhexyl)-4-bromo-1,8-naphthalimide (**1b**)[2] and **NaphtOMe**[3] were synthesized according to procedures reported in the literature.

NMR spectroscopy and high resolution mass spectrometry (HRMS)

^{1}H, ^{13}C and ^{77}Se NMR spectra were recorded on a Bruker DRX500. Chemical shifts were reported in ppm according to tetramethylsilane using the solvent residual signal as an internal reference ($CDCl_3$: δ_H = 7.26 ppm, δ_C = 77.16 ppm). Coupling constants (*J*) were given in Hz. Unless otherwise stated, NMR spectra were measured at 298 K. Resonance multiplicity was described as d (doublet), t (triplet), p (quintet), hept (heptuplet), m (multiplet), and dd (doublet of doublets). Carbon spectra were acquired with a complete decoupling for the proton. High resolution mass spectrometry (HRMS) was performed with a JEOL JMS-700 B/E spectrometer.

Absorption and emission spectroscopies

All spectroscopic measurements were performed on dilute solutions (ca 10^{-5} mol.L^{-1}) in 10 mm quartz cuvettes using spectroscopic grade solvents unless stated otherwise.

Absorption spectra were recorded on a double beam JASCO V-650 spectrometer.

Emission spectra were recorded on a Horiba-Jobin-Yvon Fluorolog-3 spectrofluorimeter equipped with a three-slit double grating excitation and emission monochromator with a dispersion of 2.1 nm/mm (1200 groove/mm) in excitation-detection geometry. A R928 photomultiplier was used as a detector. Corrections were applied for both the excitation light intensity variation and the detector spectral response. All fluorescence spectra were corrected for dark counts from the detector.

Fluorescence quantum yields were measured in spectroscopic grade chloroform using the relative method. Briefly, emission spectra were acquired for the compound of interest and the reference using the same excitation and detection parameters with an absorbance ranging from 0.1 to 0.01 at the excitation wavelength. The signal was corrected for fluctuations of the light

source intensity and detector wavelength dependent sensitivity. The area of each emission curve for the compound x and the reference ref, respectively I_x and I_{ref}, was plotted as a function of their absorbance (A_x and A_{ref}) to assess the quality of the linear correlation. The fluorescence quantum yields ϕ_x were calculated according the following equation:

$$\phi_x = \frac{A_{ref} \times I_x}{A_x \times I_{ref}} \left(\frac{n_x}{n_{ref}} \right)^2 \phi_{ref}$$

here n_x and n_{ref} are the refractive index of the solvent of the compound and reference solutions respectively, ϕ_{ref} is the fluorescence quantum yield of the reference. Coumarin 153 in ethanol, with an excitation wavelength of 375 nm was chosen as reference ($\phi_{ref} = 0.55$)

Fluorescence lifetime measurements were performed in chloroform solutions at room temperature on a Horiba-Jobin-Yvon Fluorolog-3 spectrofluorimeter, equipped with a NanoLED 390 operating at 390 nm with 250 ps pulses, a iHR320 emission monochromator with 1200 groves mm-1 gratings and a R928 photomultiplier. To obtain the Instrument Response Function, a highly diffusing colloidal silica solution (Ludox®) from Sigma-Aldrich diluted in water was used. Fluorescence lifetimes were determined by deconvolution of the acquired signal and mono-exponential (**Napht$_2$[O]**) or bi-exponential (**Napht$_2$[S]** and **Napht$_2$[Se]**) modeling of the fluorescence decay using the decay analysis software (DAS) provided

Phosphorescence spectra were measured in glassy 2-methyltetrahydrofuran solutions cooled in liquid nitrogen (77K). For non time-gated experiments, excitation and emission parameters were as described above for standard emission spectra collection. For time gated experiments excitation source was a Xe lamp in flash mode, and signal (S1c) was collected with a 60 µs delay to ensure removal of the fluorescence signal from the spectrum, with a sampling interval (integration time) of 100 µs. Excitation slits were opened at 14 nm and emission slits at 10 nm.

Singlet Oxygen quantum yields

Singlet Oxygen generation quantum yields were measured by the relative methodology, through evaluation of the singlet oxygen phosphorescence intensity of diluted chloroform solutions of the complex. Singlet-oxygen phosphorescence was recorded on a Horiba-Jobin-Yvon Fluorolog-3 spectrofluorimeter in excitation-detection geometry using a liquid nitrogen cooled, solid indium/gallium/arsenide (InGaAs) detector (850–1600 nm). The singlet oxygen

generation quantum yield $\phi_{\Delta x}$ was measured in spectroscopic grade chloroform solutions with an optical density lower than 0.1 under stirring, using the relative method. Reference was Phenalen-1-one in spectroscopic grade chloroform ($\phi_{\Delta ref} = 0.95$), and same excitation and detection parameters were used for the reference and sample measurements. The area of each emission curve for the compound x and the reference ref, respectively I_x and I_{ref}, was plotted as a function of their absorbance (A_x and A_{ref}) to assess the quality of the linear correlation. $\phi_{\Delta x}$ was calculated according to the following equation:

$$\phi_{\Delta x} = \frac{A_{ref} \times I_x}{A_x \times I_{ref}} \phi_{\Delta ref}$$

where I_x and I_{ref} are the integrated luminescence intensity of singlet oxygen for the sample and the reference, A_x and A_{ref} are the absorbance at the excitation wavelength of the sample and the reference and $\phi_{\Delta ref}$ is the singlet oxygen generation quantum yield of the reference.

S2. Syntheses

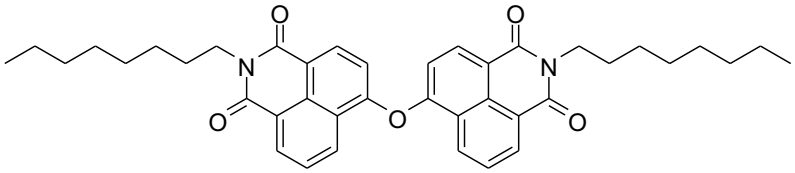

Napht$_2$[O]: A mixture of *N*-(octyl)-4-bromo-1,8-naphthalimide (6 mmol, 2.33 g), cesium fluoride (4 eq, 24 mmol, 3,65 g) and water (0.5 mL) in DMSO (50 mL) was stirred at 150°C for 1 h. The reaction mixture was cooled down to room temperature and poured into water containing 10 ml of conc. hydrochloric acid. The precipitate was filtered, washed with water and dried. The crude product was purified by column chromatography on silica (petroleum ether/dichloromethane as eluent) to afford **Napht$_2$[O]** as an off-white solid. Yield 1.01 g (53%).

^{1}H NMR (500 MHz, $CDCl_3$): δ 8.69 (dd, *J* = 7.3, 0.8 Hz, 2H), 8.58 (dd, *J* = 8.4, 0.8 Hz, 2H), 8.54 (d, *J* = 8.1 Hz, 2H), 7.81 (dd, *J* = 8.4, 7.3 Hz, 2H), 7.17 (d, *J* = 8.1 Hz, 2H), 4.18 (t, *J* = 7.6 Hz, 4H), 1.73 (p, *J* = 7.6 Hz, 4H), 1.47 – 1.21 (m, 20H), 0.87 (t, *J* = 6.9 Hz, 6H). ^{13}C NMR (125 MHz, $CDCl_3$): δ 164.13, 163.51, 157.45, 132.48, 132.31, 130.02, 127.98, 127.51, 124.51, 123.29, 119.24, 114.44, 40.71, 31.95, 29.47, 29.36, 28.28, 27.28, 22.77, 14.22. HRMS calcd. for $C_{40}H_{43}N_2O_5$ ($[M-H]^-$): 631.3178, found: 631.3183.

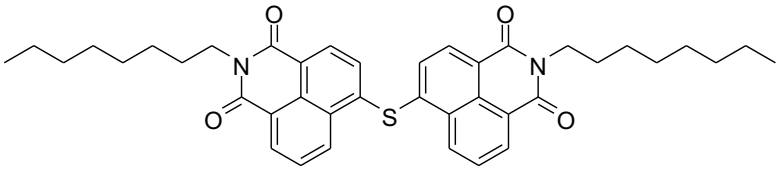

Napht$_2$[S]: A mixture of *N*-(octyl)-4-bromo-1,8-naphthalimide (8 mmol, 3.11 g), sodium sulfide hydrate (1.80 g) in DMSO (50 mL) was stirred at 110°C for 1.5 h. The reaction mixture was cooled down to room temperature and poured into water containing 10 ml of conc. hydrochloric acid. The precipitate was filtered, washed with water and dried. The crude product was purified by column chromatography on silica (petroleum ether/dichloromethane as eluent) to afford **Napht$_2$[S]** as a yellowish solid. Yield 1.27 g (49%).

^{1}H NMR (500 MHz, $CDCl_3$): δ 8.66 (m, 4H), 8.41 (d, *J* = 7.7 Hz, 2H), 7.80 (dd, *J* = 8.4, 7.4 Hz, 2H), 7.50 (d, *J* = 7.7 Hz, 2H), 4.16 (t, *J* = 7.6 Hz, 4H), 1.72 (p, *J* = 7.6 Hz, 4H), 1.45 – 1.19 (m, 20H), 0.86 (t, *J* = 6.9 Hz, 6H). ^{13}C NMR (125 MHz, $CDCl_3$): δ 163.81, 163.66, 139.49, 132.08, 130.88, 130.85, 130.64, 130.60, 128.98, 128.00, 123.74, 122.74, 40.78, 31.95, 29.46, 29.35, 28.25, 27.28, 22.77, 14.22. HRMS calcd. for $C_{40}H_{45}N_2O_4S$ ($[M+H]^+$): 649.3095, found: 649.3088.

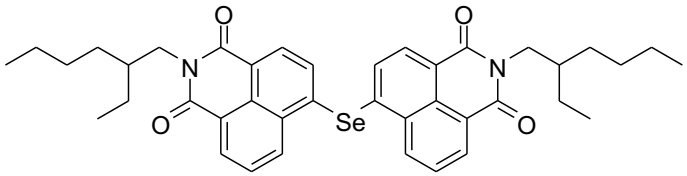

Napht$_2$[Se]: To a suspension of powdered selenium (6 mmol, 0.48 g) in dry NMP (50 ml), a small piece of sodium (6 mmol, 0.14 g) was added. The suspension was stirred at 140°C for 1 h. The reaction mixture was cooled to 90°C and solid *N*-(2-ethylhexyl)-4-bromo-1,8-naphthalimide (8 mmol, 3.11 g) was added in one portion. The reaction mixture was stirred at 90°C for 1 h and poured into water containing 10 ml of conc. hydrochloric acid. The precipitate was filtered, washed with water and dried. The crude product was purified by column chromatography on silica (petroleum ether/dichloromethane as eluent) to afford **Napht$_2$[Se]** as a yellowish solid. Yield 1.70 g (61%).

^{1}H NMR (500 MHz, $CDCl_3$): δ 8.66 (dd, *J* = 7.5, 0.7 Hz, 2H), 8.59 (dd, *J* = 8.3, 0.7 Hz, 2H), 8.36 (d, *J* = 7.7 Hz, 2H), 7.80 (dd, *J* = 8.3, 7.5 Hz, 2H), 7.69 (d, *J* = 7.7 Hz, 2H), 4.11 (m, 4H), 1.93 (hept, *J* = 6.1 Hz, 2H), 1.44 – 1.22 (m, 16H), 0.95 – 0.82 (m, 12H). ^{13}C NMR (125 MHz, $CDCl_3$): δ 164.18, 164.16, 137.63, 133.01, 132.57, 132.11, 131.92, 131.01, 128.95, 128.08,

123.73, 123.14, 44.42, 38.07, 30.86, 28.81, 24.17, 23.22, 14.24, 10.77. ^{77}Se NMR (95 MHz, $CDCl_3$): δ 345.34. HRMS calcd. for $C_{40}H_{43}N_2O_4Se$ ([M−H]$^-$): 695.2394, found: 695.2417.

S3. NMR spectra

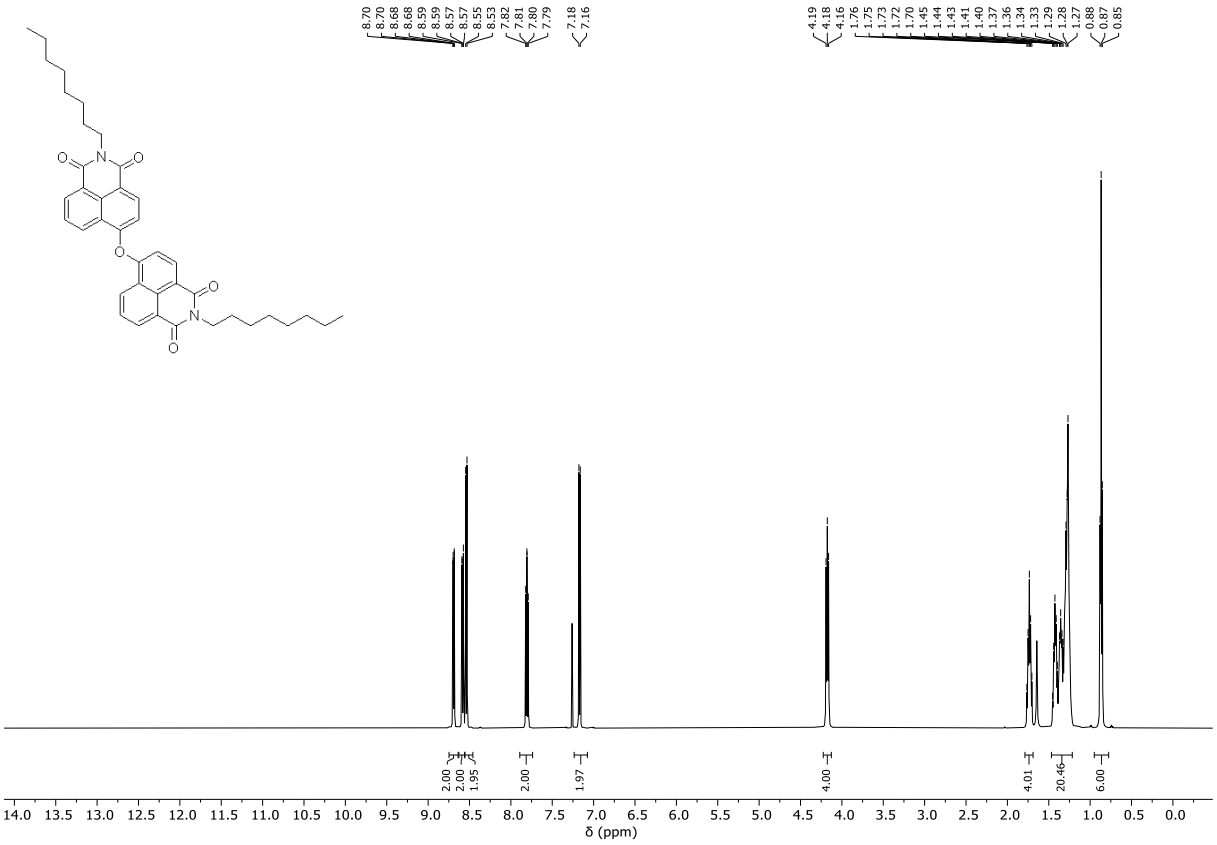

Figure S1. ^{1}H NMR (500 MHz, $CDCl_3$) spectrum of **Napht$_2$[O]**.

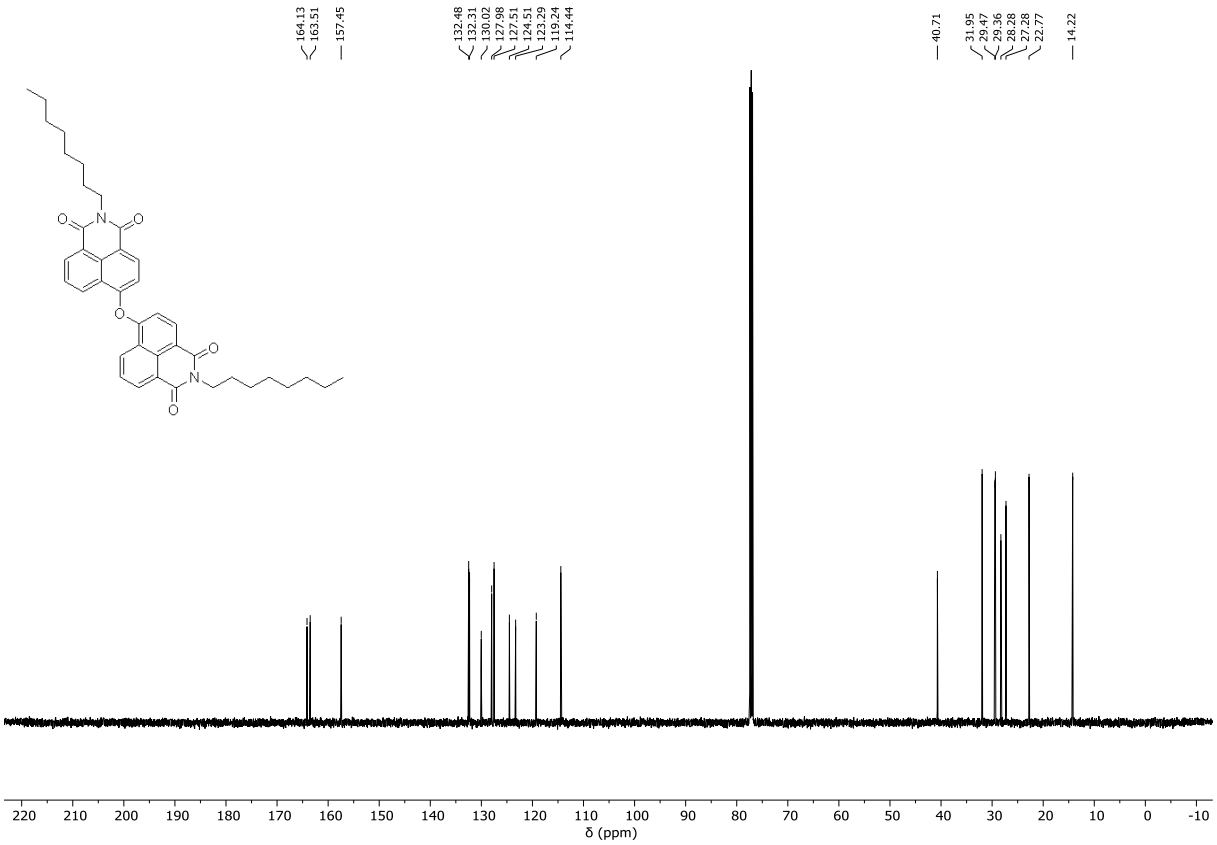

Figure S2. ^{13}C NMR (125 MHz, $CDCl_3$) spectrum of $Napht_2[O]$.

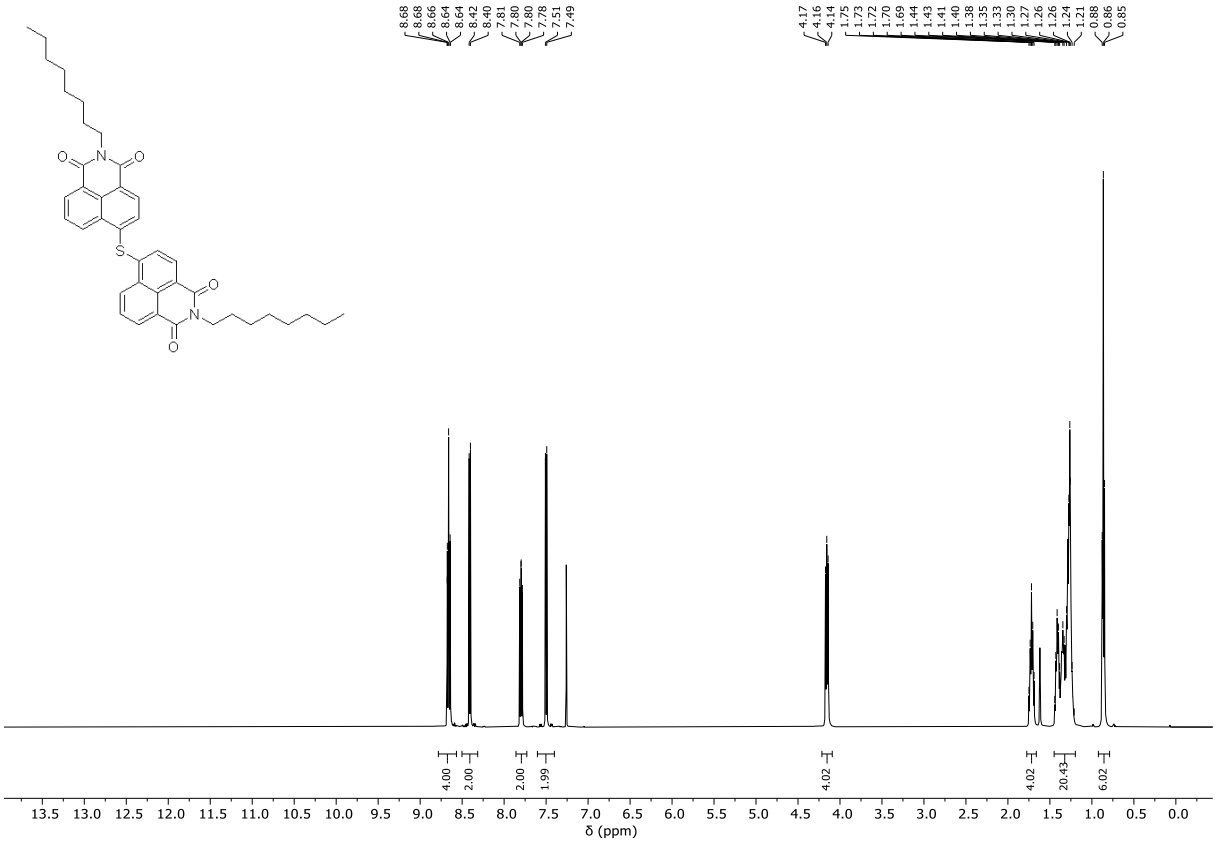

Figure S3. ^{1}H NMR (500 MHz, $CDCl_3$) spectrum of **$Napht_2$[S]**.

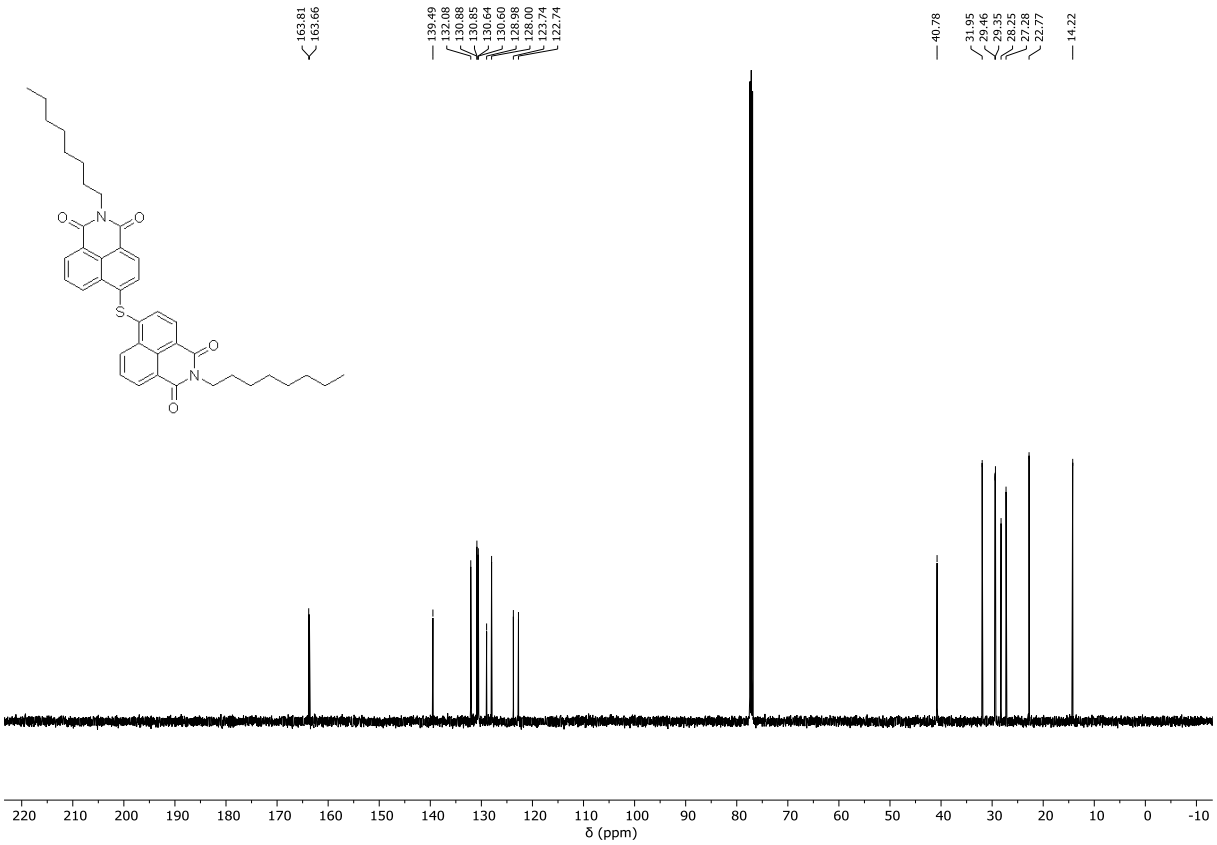

Figure S4. ^{13}C NMR (125 MHz, $CDCl_3$) spectrum of **Napht$_2$[S]**.

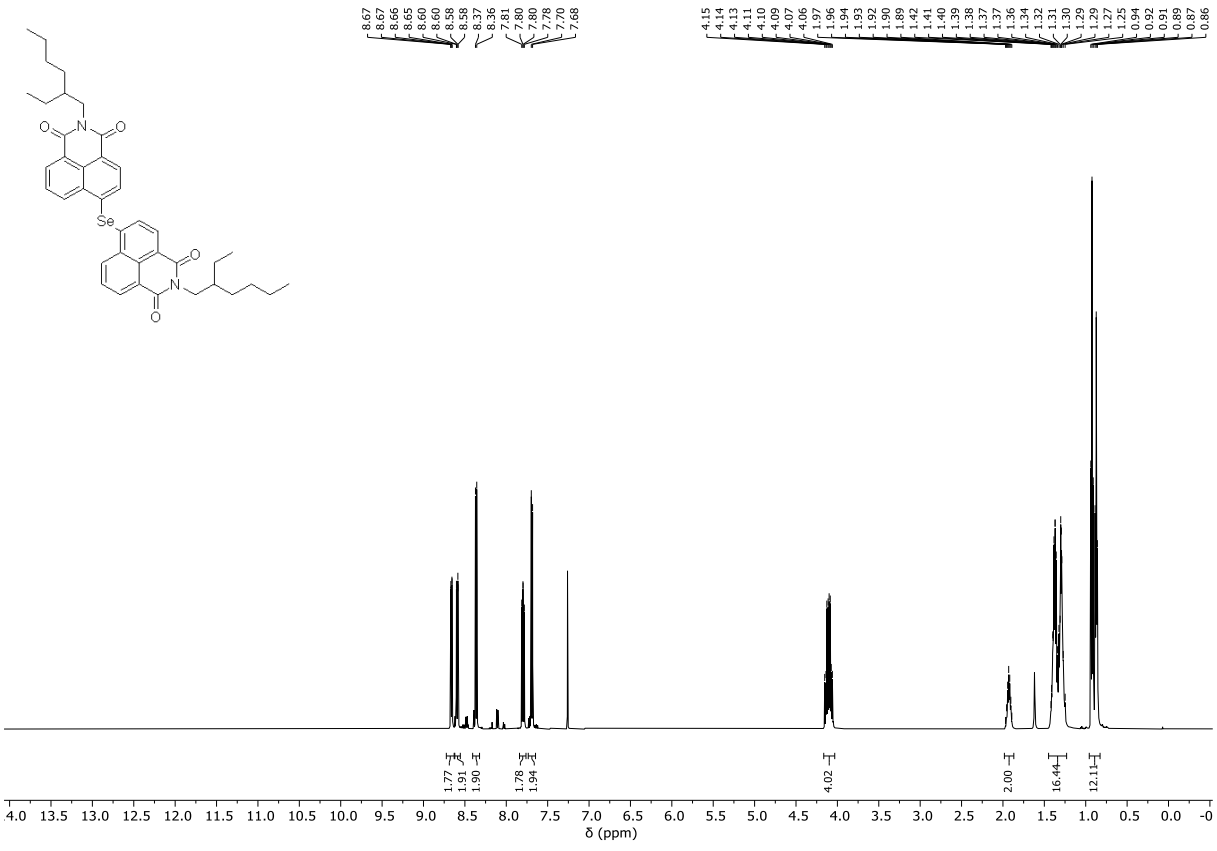

Figure S5. ^{1}H NMR (500 MHz, $CDCl_3$) spectrum of **Napht$_2$[Se]**.

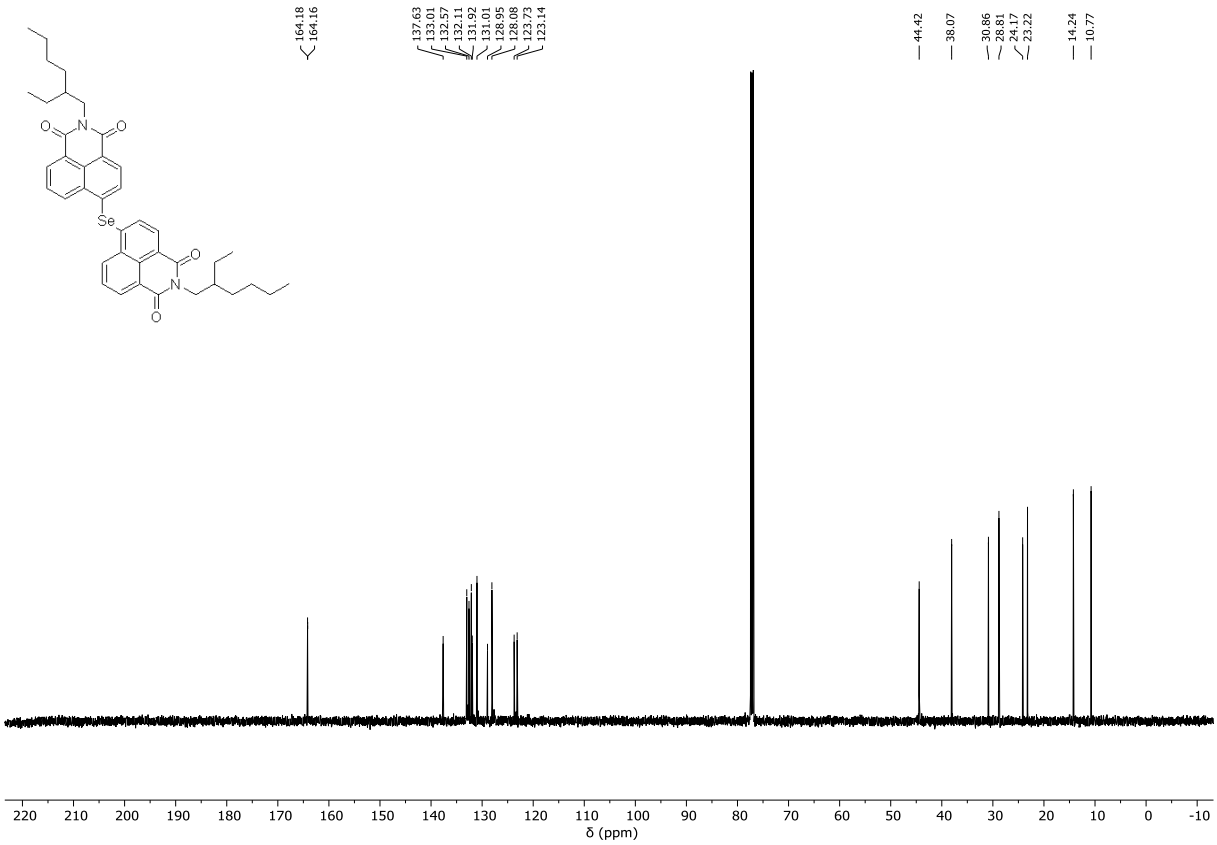

Figure S6. ^{13}C NMR (125 MHz, $CDCl_3$) spectrum of **Napht$_2$[Se]**.

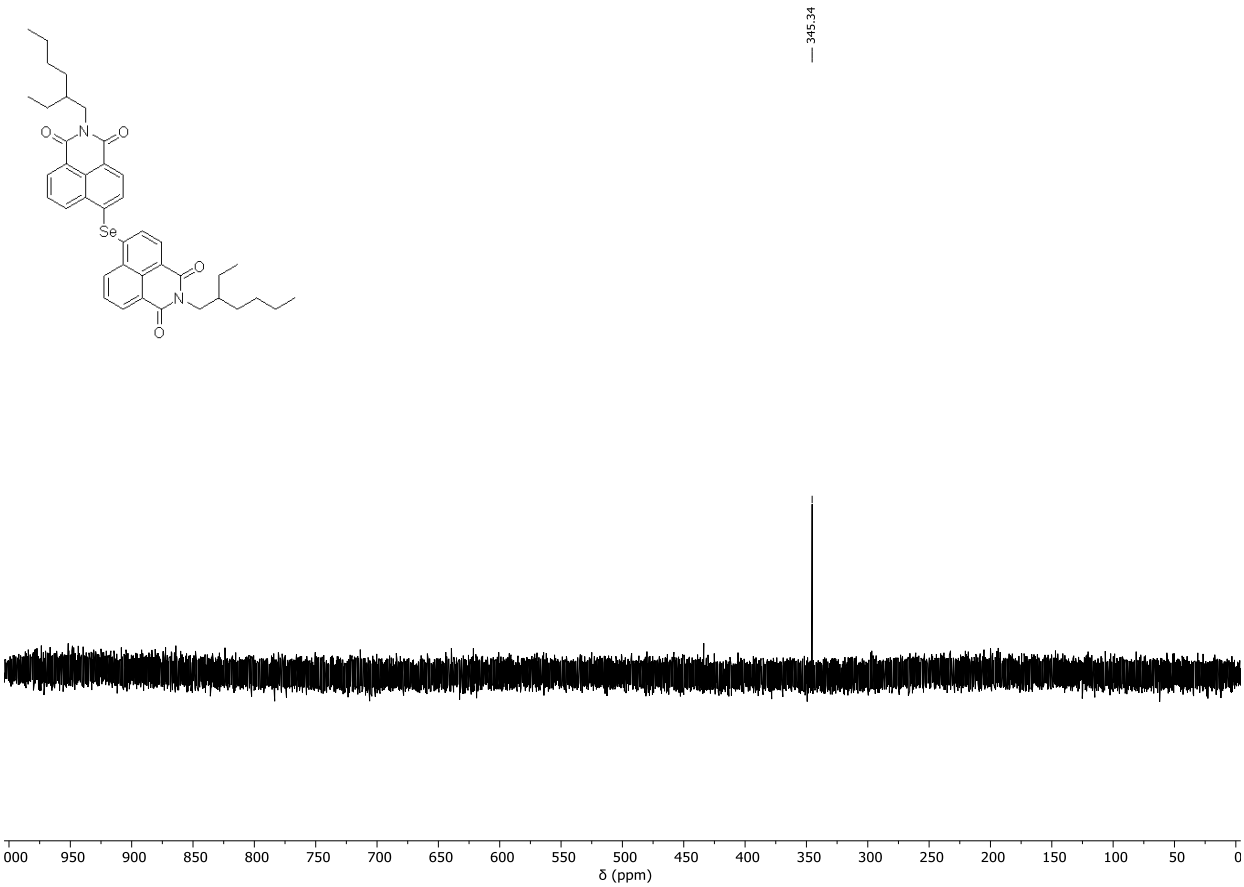

Figure S7. ^{77}Se NMR (95 MHz, $CDCl_3$) spectrum of **Napht$_2$[Se]**.

S4. HRMS spectra

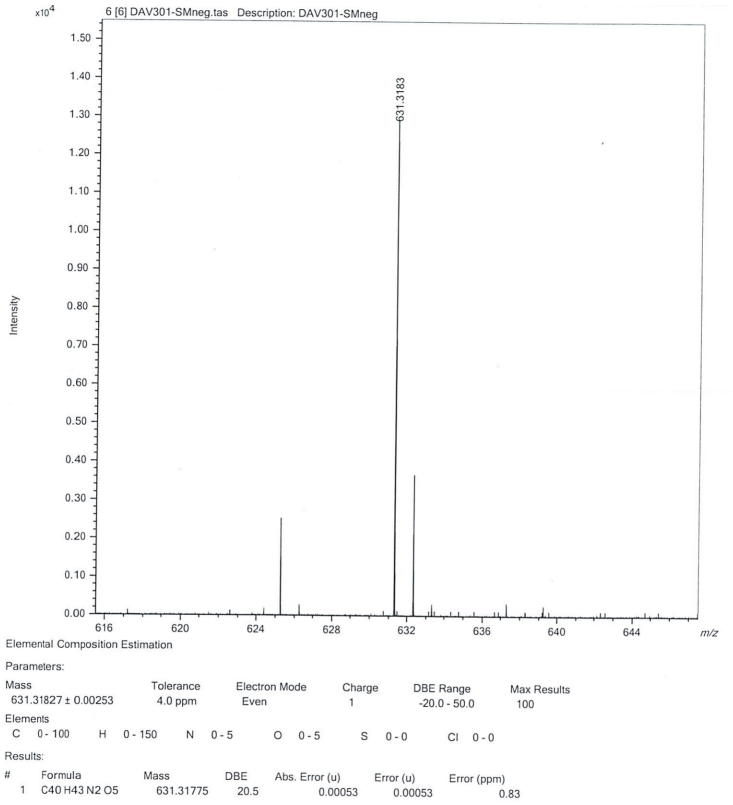

Figure S8. HRMS spectrum of **Napht$_2$[O]**.

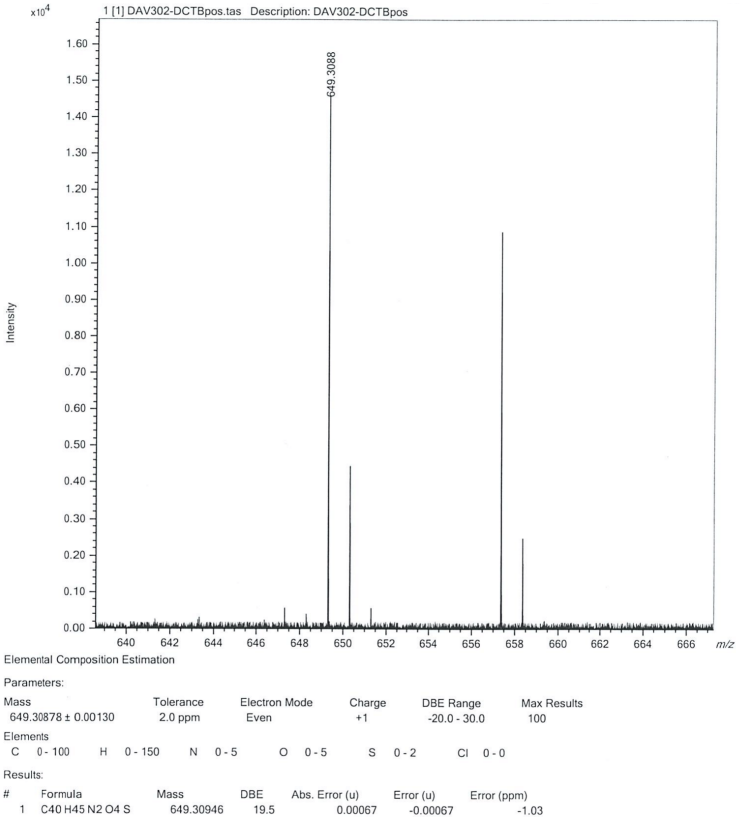

Figure S9. HRMS spectrum of **Napht$_2$[S]**.

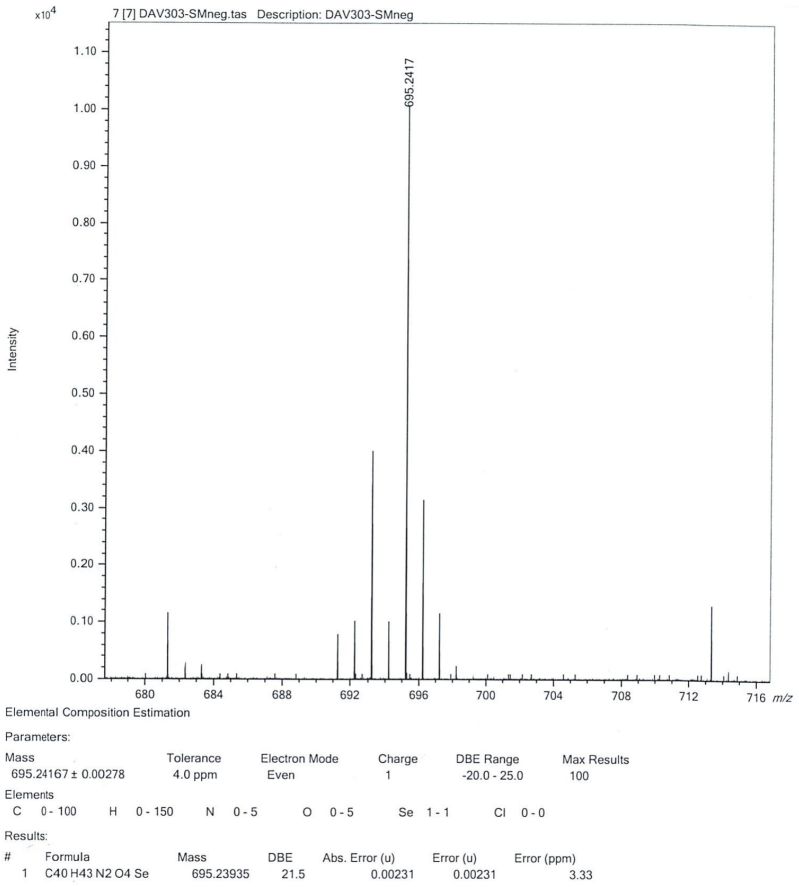

Figure S10. HRMS spectrum of **Napht$_2$[Se]**.

S5. Spectroscopy

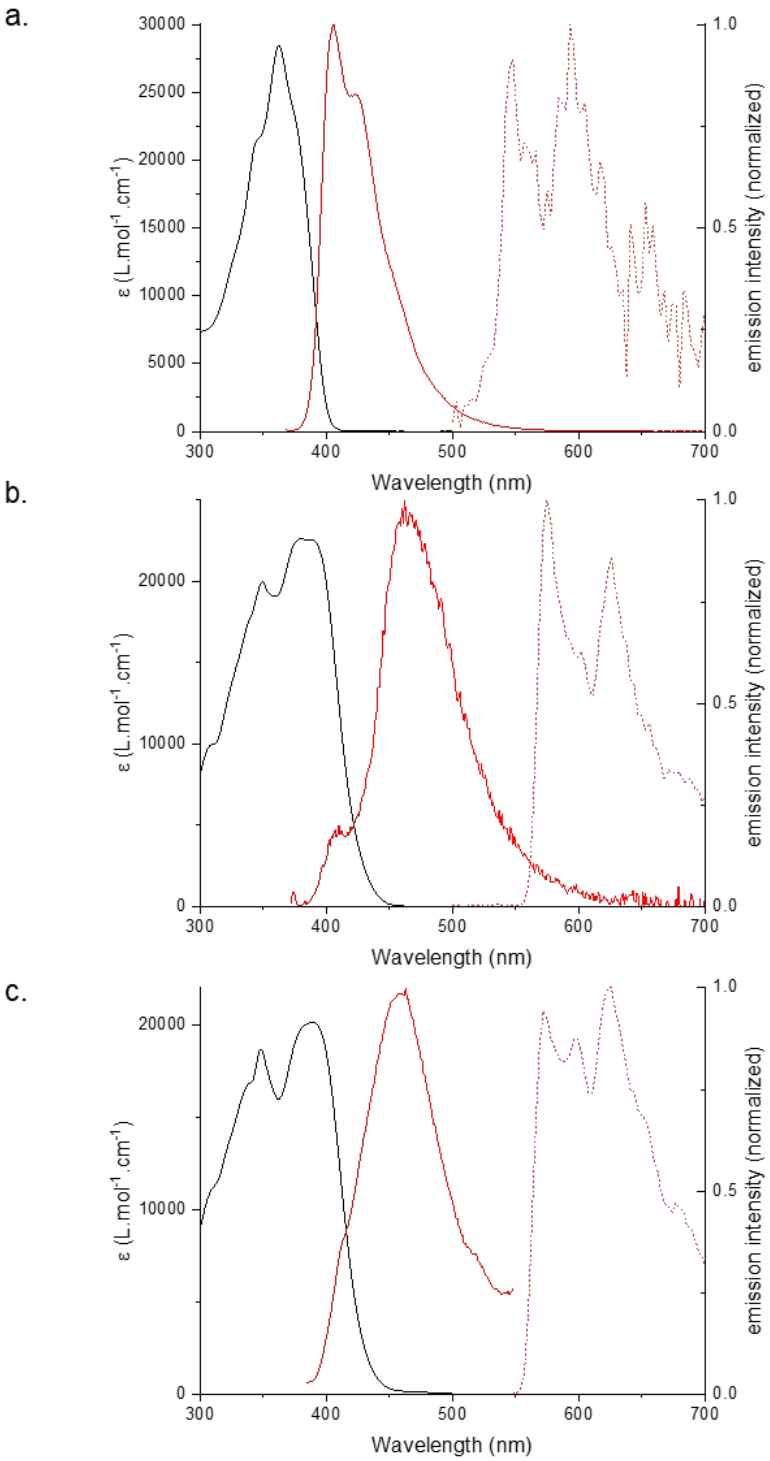

Figure S11. Absorption (black), normalized emission (red, full) and 77K phosphorescence (red, dashed) spectra of: a. **Napht$_2$[O]** (black), b. **Napht$_2$[S]**, and c. **Napht$_2$[Se]** (blue).

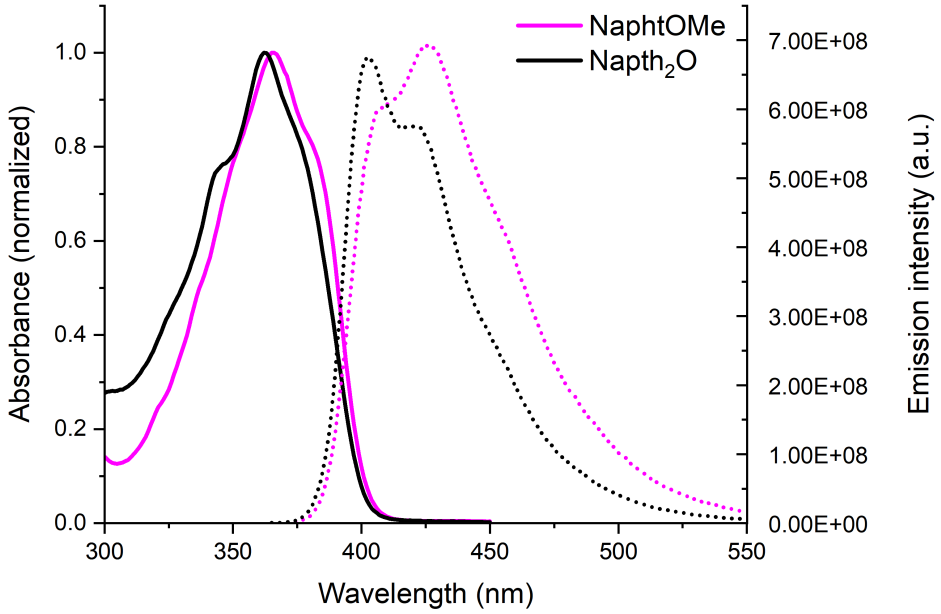

Figure S12. Normalized absorption (full) and emission at iso-absorbance (dashed; excitation wavelength: 350 nm) spectra of Napht$_2$[O] (black) and NaphtOMe (magenta).

Dependence of the absorption spectra on concentration

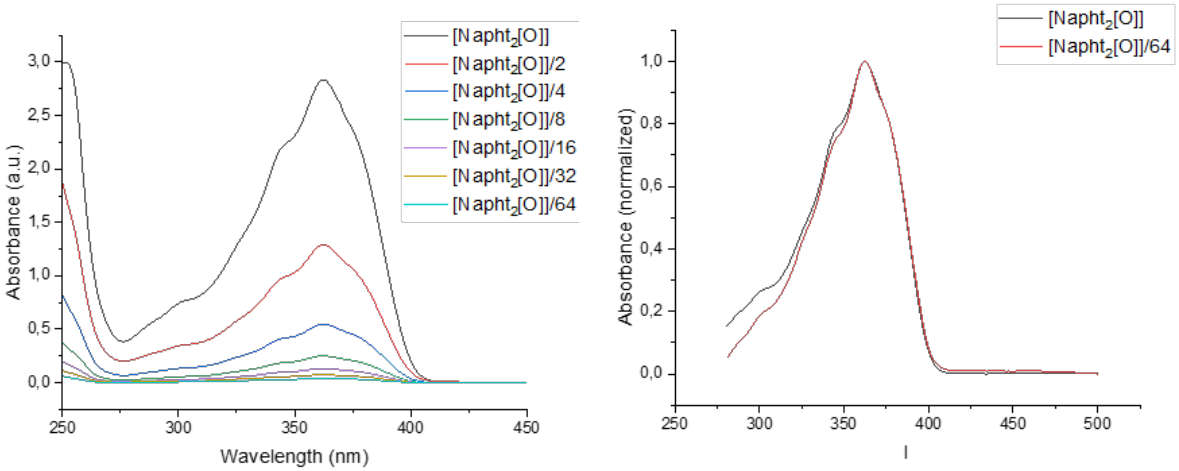

Figure S13. (left) spectra of successive 2-fold dilutions of compound **Napht$_2$[O]** in chloroform (right) normalized spectra of the two extrema, minor deviations are most likely due to baseline correction issues.

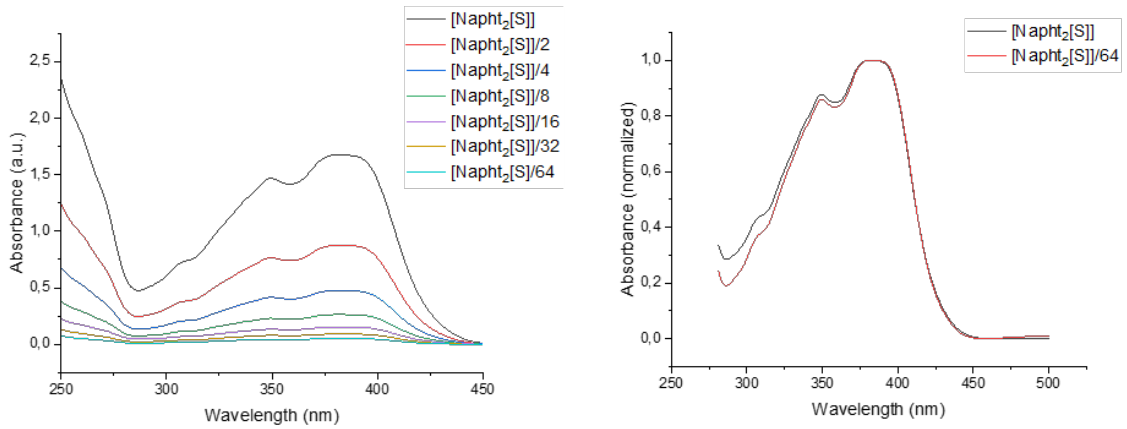

Figure S14. (left) spectra of successive 2-fold dilutions of compound **Napht$_2$[S]** in chloroform (right) normalized spectra of the two extrema, minor deviations are most likely due to baseline correction issues.

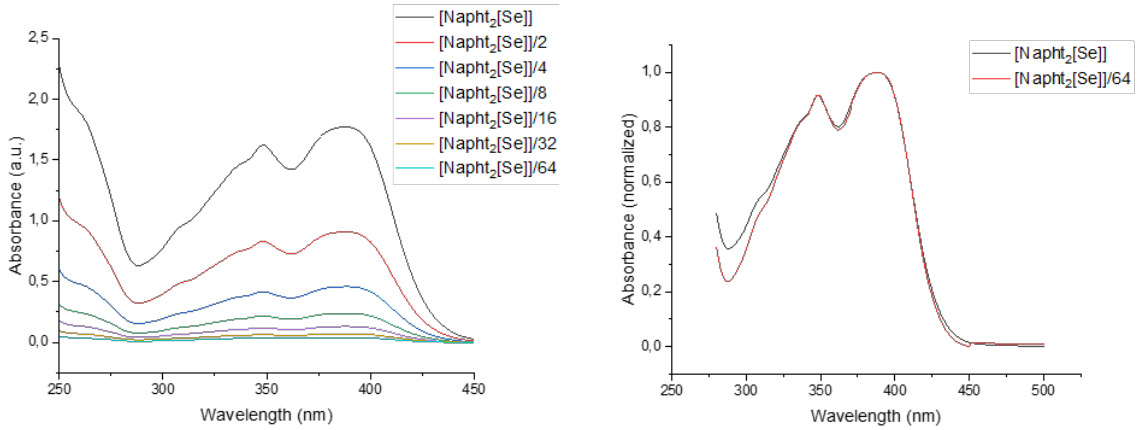

Figure S15. (left) spectra of successive 2-fold dilutions of compound **Napht$_2$[Se]** in chloroform (right) normalized spectra of the two extrema, minor deviations are most likely due to baseline correction issues.

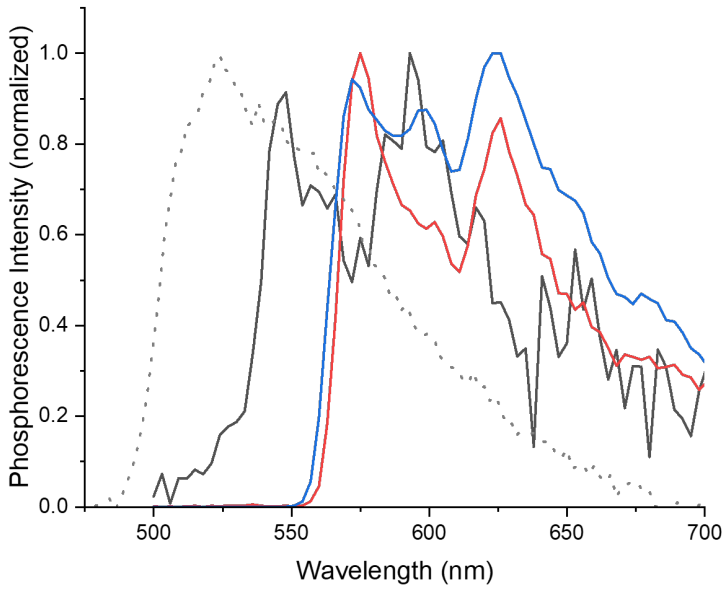

Figure S16. Phosphorescence spectra recorded in 2-Methyltetrahydrofuran at 77K with a time gate of 50µs. **Napht2[O]** (black, full); **Napth2[S]** (red, full); **Napht2[Se]** (blue, full), **NaphtOMe** (grey, dashed).

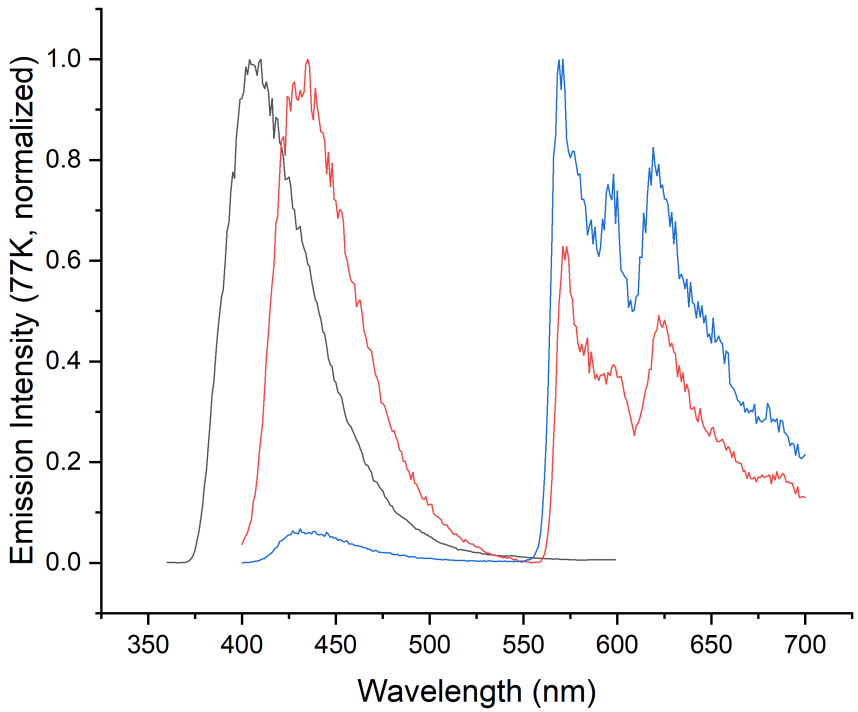

Figure S17. Phosphorescence spectra recorded in 2-Methyltetrahydrofuran at 77K without time gate of 50µs**. Napht2[O]** (black, full); **Napth2[S]** (red, full); **Napht2[Se]** (blue, full).

Singlet oxygen quantum yield measurements

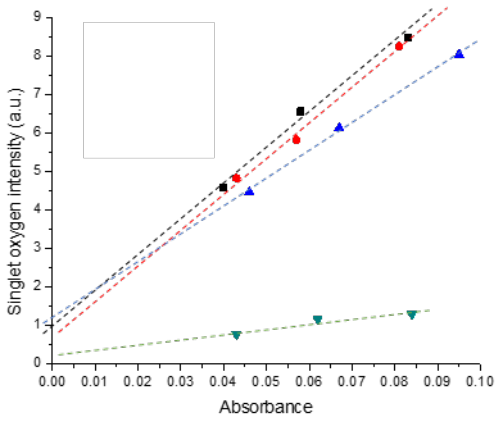

Figure S18. Singlet oxygen phosphorescence intensity vs absorbance for $CDCl_3$ solutions of **Napht$_2$[O]** (green down triangles) **Napht$_2$[S]** (red circles) **Napht$_2$[Se]** (blue up triangles) and reference compound phenalene-1-one (black squares; φ_Δ=0.97 in chloroform).

Theoretical Calculations

S6. Computational Methods

Ground and excited state geometries were optimized using time-dependent density functional theory (TDDFT) within the Tamm-Dancoff approximation (TDA)[4] with the CAM-B3LYP[5] functional in combination with D4 dispersion corrections[6]. The basis set selected for optimizations was def2-SVP basis set together with RI-J auxiliary basis and RIJCOSX approximation which were used in all calculations. Vibrational frequency analyses were performed at the same level to verify that all optimized structures correspond to true minima on the potential energy surface. Single point energy calculations were carried out with the def2-TZVP basis set (plus auxiliary basis sets as described above) on the optimized geometries. Tight numerical integration grids (DefGrid3) were employed. Solvent effects were included using the polarizable continuum model (PCM)[7] with chloroform as the implicit solvent, unless otherwise specified. All DFT and TDDFT calculations were done using Orca Program version 6.0.0.[8]

Single point energies were also computed using the second-order approximate coupled-cluster (CC2)[9] method. The CC2 excitation energies were computed in the gas phase at the TDA-DFT optimized geometries. The def2-TZVP basis set was used along with the resolution identity approximation. Solvent effects on the CC2 excitation energies were estimated by applying a correction term corresponding to the energy difference between the gas-phase and

CPCM/chloroform calculated with TDA/CAM-B3LYP-D4/def2-TZVP. Turbomole v.7.8[10, 11] was used to perform CC2 calculations.

Spin–orbit coupling (SOC) matrix elements were computed as implemented in the ORCA package, using the TDA wavefunctions. SOC between the lowest singlets and triplets were computed at the S_1 optimized geometry using the Douglas–Kroll Hamiltonian along with the spin-orbit mean field approach. These calculations use the same basis sets as specified for the single point calculations above.

The wave function analyses were done using the TheoDORE[12] package. Natural transition orbitals (NTOs) and descriptors such as charge-transfer (CT) numbers, participation ratios (PR) based on transition density matrices were investigated to allow the characterization of the excited states in terms of local excitation, charge-transfer, excitonic resonance, or charge resonance character. Electron density difference plots were done using Orca and visualized using Chimera program.

Absorption and emission spectra for the dimers and monomers were sampled using Nuclear Ensemble approach[13]. Geometries were sampled from a harmonic oscillator Wigner distribution of the nuclei at a temperature of 0 K, using the normal modes and vibrational frequencies at each equilibrium geometry calculated at the equilibrium geometry level (TDA-CAM-B3LYP-D4/def2-SVP). To this end, 500 single point calculations were computed at the TDA/CAM-B3LYP-D4/def2-TZVP level (including the approximations for the basis set mentioned above and Chloroform as solvent) using ORCA program interfaced with NewtonX-CS[14]. The spectrum at 0K was convoluted using the vertical excitations, with a Gaussian function with a broadening of 0.045 eV (delta) eV and 0.005 eV as a distance between consecutive points (eps), and kappa = 0.

S7. Supplementary Computational results

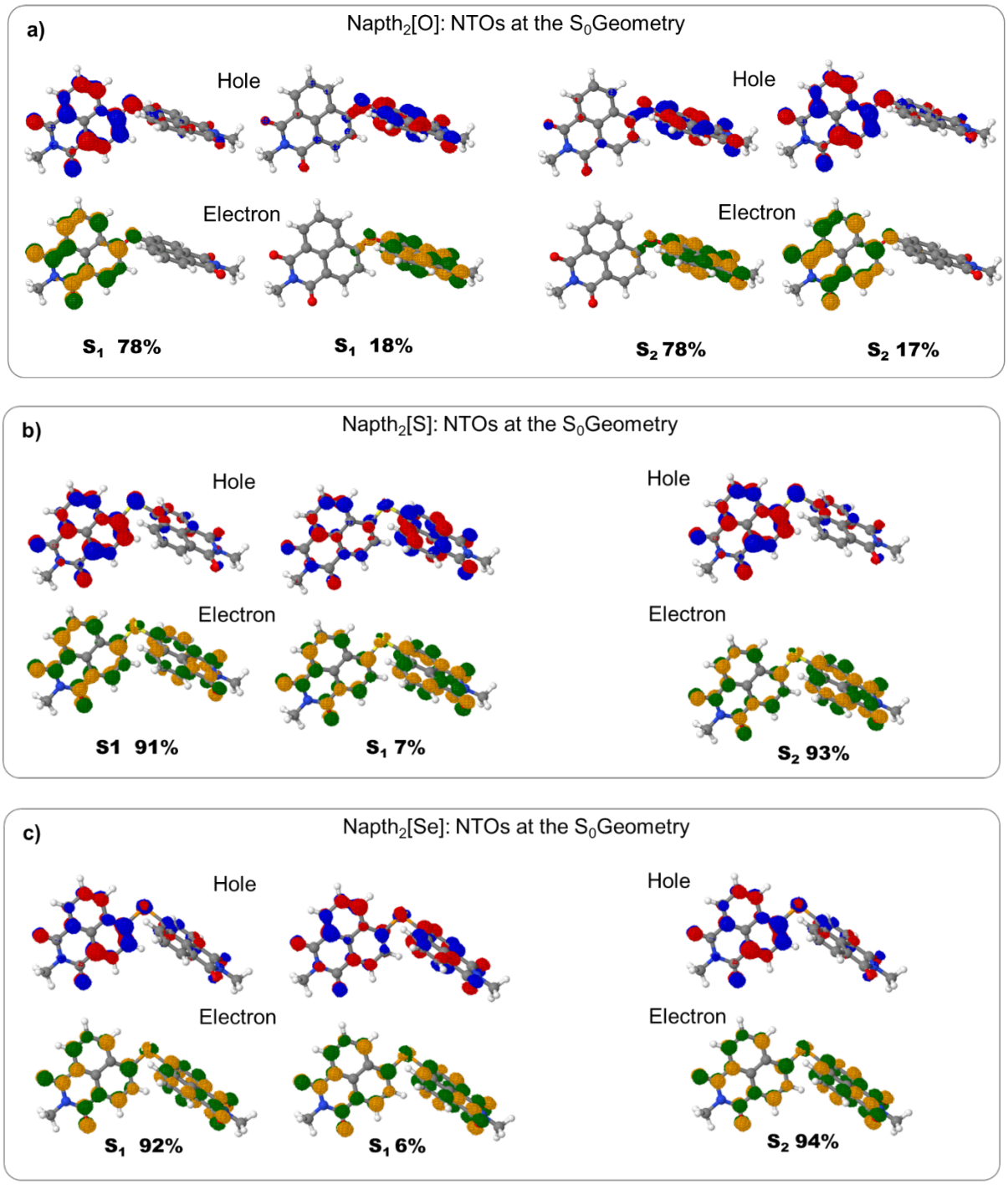

Figure S19. Natural transition orbitals (NTOs) and main composition for the $S_0 \rightarrow S_1$ and $S_0 \rightarrow S_2$ vertical transitions from the ground state minimum.

Table S1. Energy gaps between the S_1 (at its minimum) and the three lowest triplet states calculated at CC2 and TDDFT levels. Spin-orbit couplings calculated at the TDDFT level. Solvent effects (PCM/Chloroform) are included.

	Napht$_2$[O]			**Napth$_2$[S]**			**Napht$_2$[Se]**		
States	**ΔE (eV) (CC2)**	**ΔE (eV) (TDDFT)**	**SOC (cm^{-1})**	**ΔE (eV) (CC2)**	**ΔE (eV) (TDDFT)**	**SOC (cm^{-1})**	**ΔE (eV) (CC2)**	**ΔE (eV) (TDDFT)**	**SOC (cm^{-1})**
S_1-T_1	-1.03	-1.09	0.36	-0.83	-0.88	3.02	-0.77	-0.86	20.24
S_1-T_2	-0.94	-1.02	1.01	-0.66	-0.72	5.18	-0.60	-0.69	20.96
S_1-T_3	0.15	0.14	1.03	0.163	0.21	3.27	0.12	0.14	12.46

Table S2. Calculated vertical absorption and emission energies and respective oscillator strengths for the monomers at the TDDFT level in PCM/chloroform.

	State	**E_{vert} (eV) (absorption)**	***f***	**E_{vert} (eV) (emission)**	***f***
Napht[O]Me	S_1	3.83	0.545	3.36	0.533
	S_2	4.39	0.019	4.26	0.010
	T_1	2.61		2.14	
	T_2	3.71		3.47	
Napht[S]Me	S_1	3.57	0.622	3.14	0.635
	S_2	4.29	0.040	4.16	0.030
	T_1	2.48		2.02	
	T_2	3.56		3.27	
Napht[Se]Me	S_1	3.49	0.580	3.07	0.607
	S_2	4.28	0.045	4.15	0.037
	T_1	2.49		2.04	
	T_2	3.53		3.22	

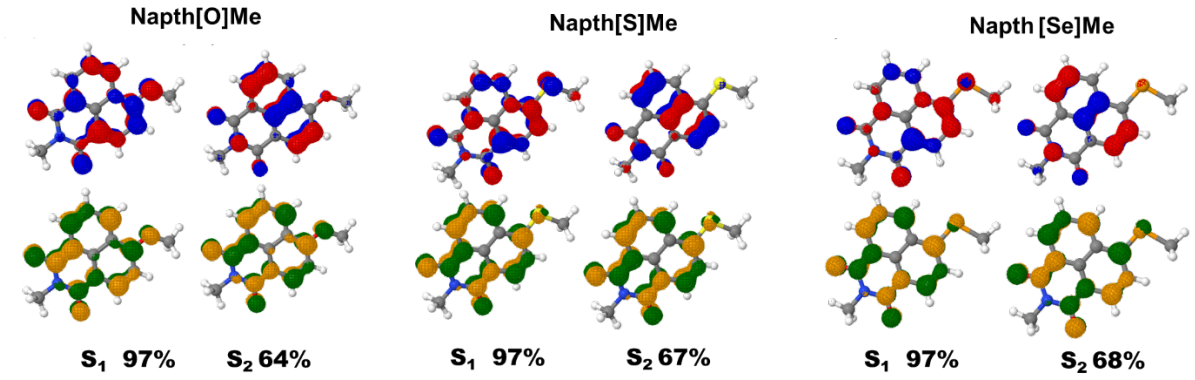

Figure S20. Natural transition orbitals (NTOs) and main composition for the S_1 and S_2 states at the minimum of the S_1 geometry. The hole is represented in red and blue; the electron is represented in yellow and green. The corresponding states at the S_0 geometry are equivalent, having also similar values for the contribution for each state.

Table S3. Energy gaps between the S_1 (at its minimum) and the three lowest triplet states calculated at CC2 and TDDFT levels. Spin-orbit couplings calculated at the TDDFT level. Solvent effects (PCM/Chloroform) are included.

	Napht[O]Me		**Napht[S]Me**		**Napht[Se]Me**	
States	**ΔE (eV) (TDDFT)**	**SOC (cm^{-1})**	**ΔE (eV) (TDDFT)**	**SOC (cm^{-1})**	**ΔE (eV) (TDDFT)**	**SOC (cm^{-1})**
S_1-T_1	-1.22	0.00	-1.12	0.00	-1.03	0.10
S_1-T_2	0.11	0.02	0.13	0.02	0.15	0.18
S_1-T_3	0.38	0.02	0.47	0.02	0.51	0.16

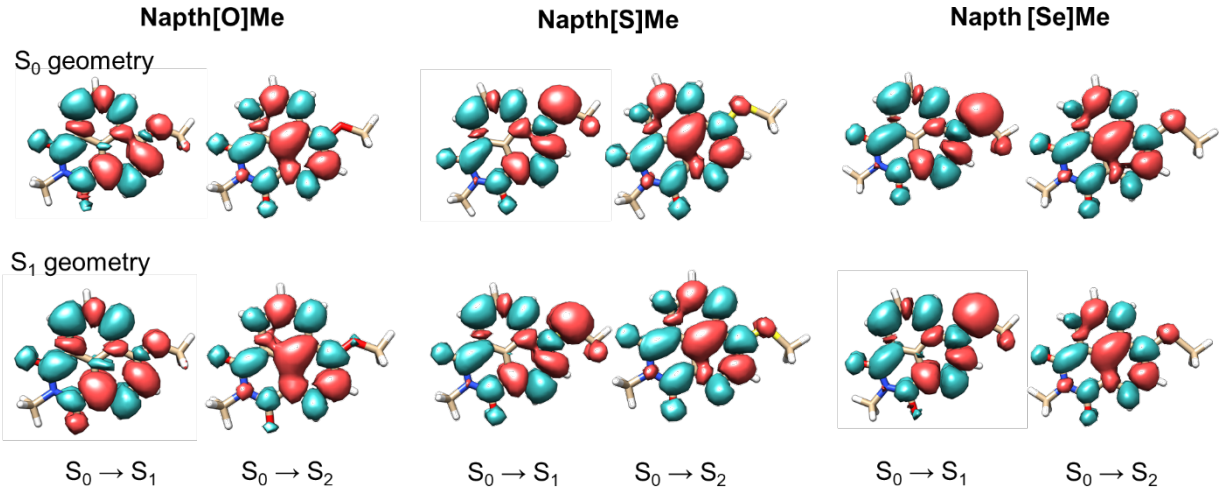

Figure S21. Electron density difference between S_0 and S_1 and S_0 and S_2 at the geometry of the ground and first excited singlet state calculated for the monomers.

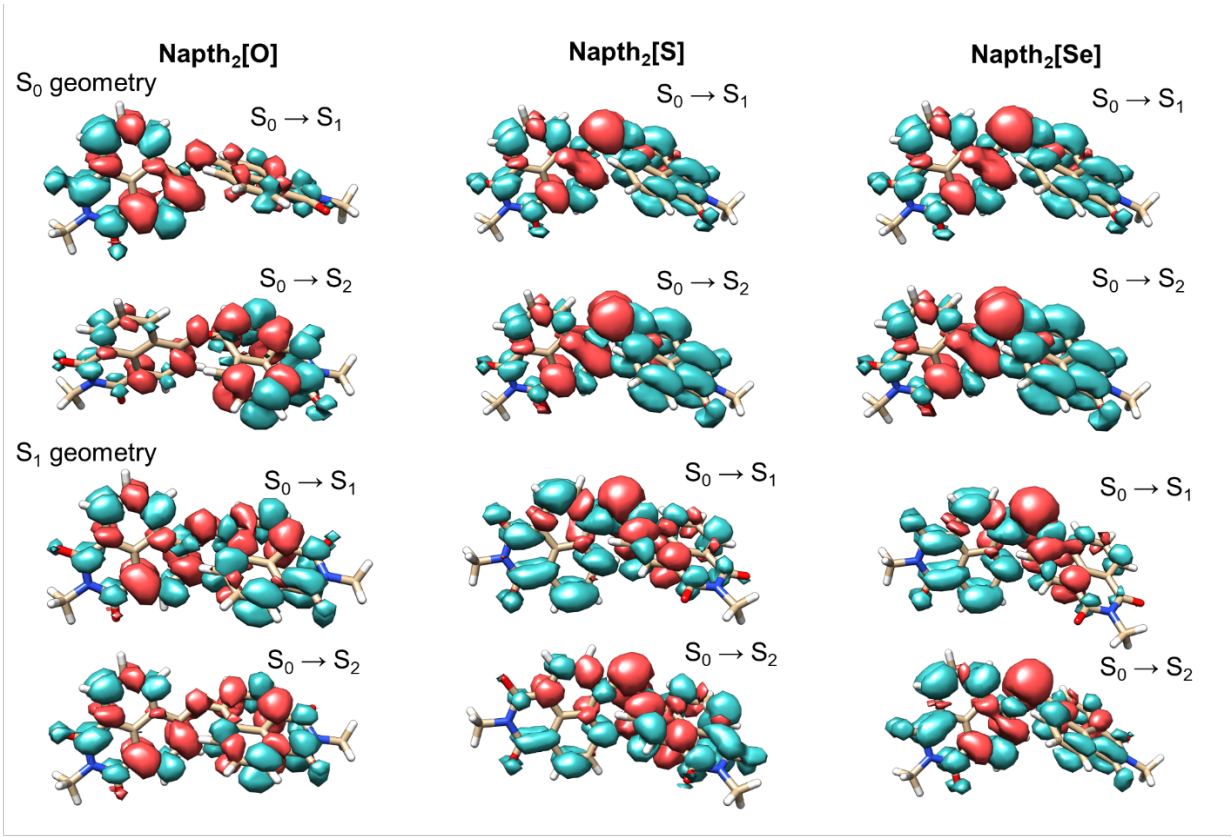

Figure S22. Electron density difference between S_0 and S_1 and S_0 and S_2 at the geometry of the ground and first excited singlet state calculated for the dimers.

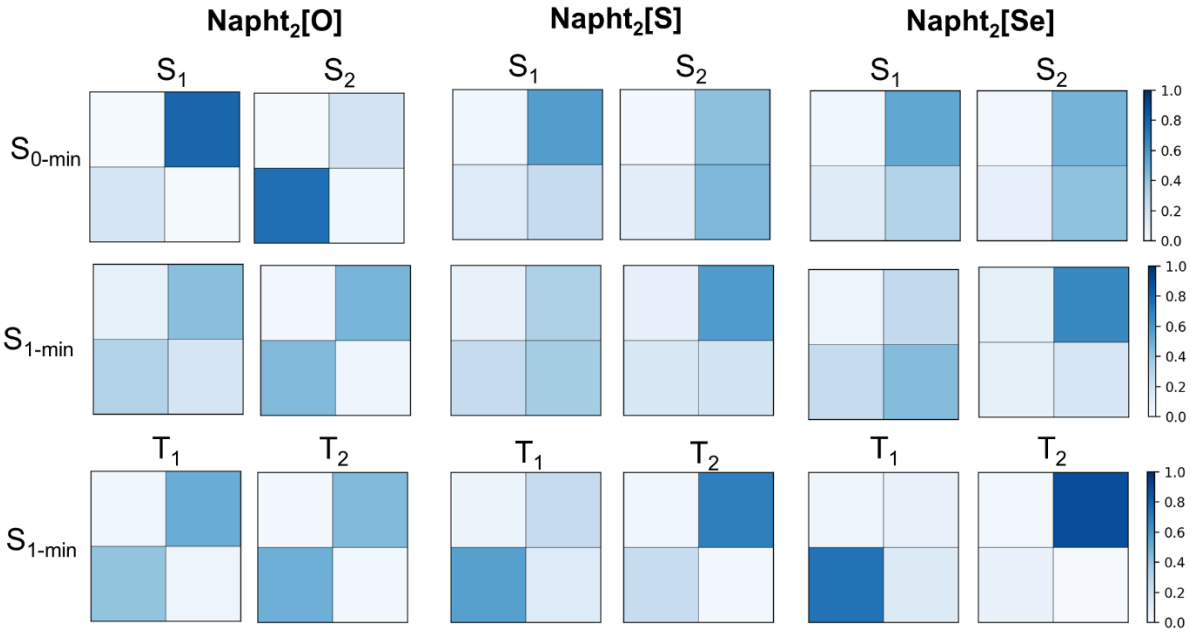

Figure S23. Electron-hole correlation plots of the Omega matrices for the individual states of the dimers.

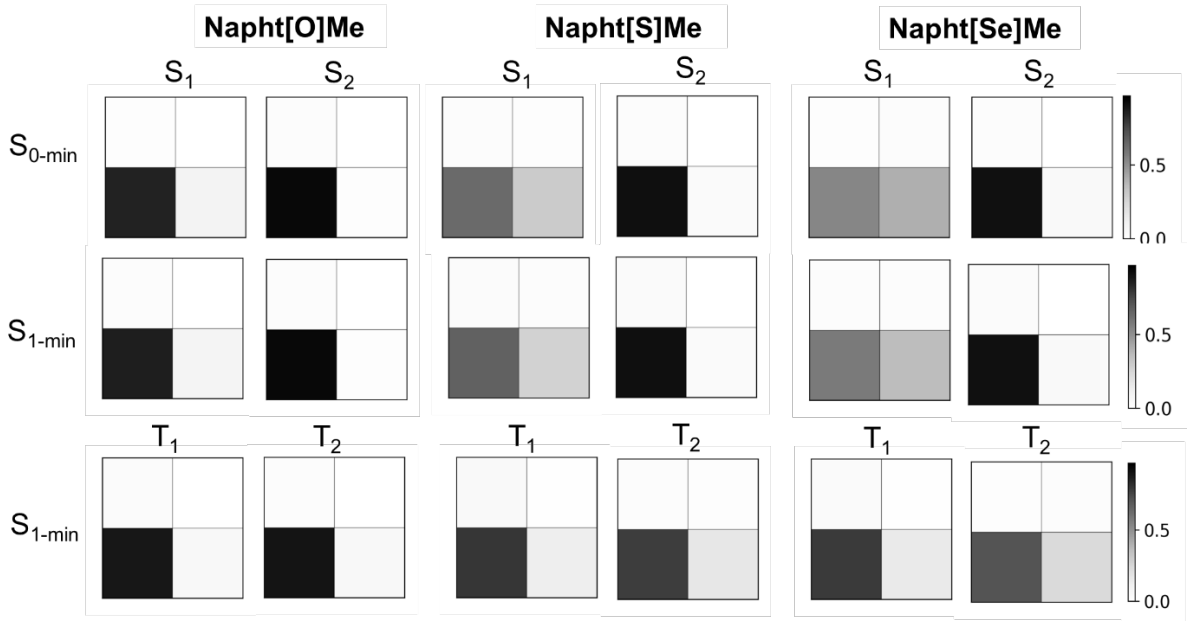

Figure S24. Electron-hole correlation plots of the Omega matrices for the individual states of the monomers.

S8. Supplementary References

1. Z. Chen, X. Liang, H. Zhang, H. Xie, J. Liu, Y. Xu, W. Zhu, Y. Wang, X. Wang, S. Tan, D. Kuang and X. Qian, *J. Med. Chem.*, 2010, **53**, 2589-2600.
2. P. de Echegaray, M. J. Mancheño, I. Arrechea-Marcos, R. Juárez, G. López-Espejo, J. T. López Navarrete, M. M. Ramos, C. Seoane, R. P. Ortiz and J. L. Segura, *The Journal of Organic Chemistry*, 2016, **81**, 11256-11267.
3. X. Zhang, Z. Wang, Y. Hou, Y. Yan, J. Zhao and B. Dick, *J. Mater. Chem. C*, 2021, **9**, 11944-11973.
4. E. Runge and E. K. U. Gross, *Phys. Rev. Lett.*, 1984, **52**, 997-1000.
5. T. Yanai, D. P. Tew and N. C. Handy, *Chem. Phys. Lett.*, 2004, **393**, 51-57.
6. E. Caldeweyher, C. Bannwarth and S. Grimme, *J. Chem. Phys.*, 2017, **147**, 034112.
7. V. Barone and M. Cossi, *J. Phys. Chem. A*, 1998, **102**, 1995-2001.
8. B. de Souza, G. Farias, F. Neese and R. Izsák, *Journal of Chemical Theory and Computation*, 2019, **15**, 1896-1904.
9. O. Christiansen, H. Koch and P. Jørgensen, *Chem. Phys. Lett.*, 1995, **243**, 409-418.
10. S. G. Balasubramani, G. P. Chen, S. Coriani, M. Diedenhofen, M. S. Frank, Y. J. Franzke, F. Furche, R. Grotjahn, M. E. Harding, C. Hättig, A. Hellweg, B. Helmich-Paris, C. Holzer, U. Huniar, M. Kaupp, A. Marefat Khah, S. Karbalaei Khani, T. Müller, F. Mack, B. D. Nguyen, S. M. Parker, E. Perlt, D. Rappoport, K. Reiter, S. Roy, M. Rückert, G. Schmitz, M. Sierka, E. Tapavicza, D. P. Tew, C. van Wüllen, V. K. Voora, F. Weigend, A. Wodyński and J. M. Yu, *J. Chem. Phys.*, 2020, **152**, 184107.
11. *Journal*.
12. F. Plasser, *J. Chem. Phys.*, 2020, **152**, 084108.
13. R. Crespo-Otero and M. Barbatti, *Theor. Chem. Acc.*, 2012, **131**, 1237.

14. M. Barbatti, M. Bondanza, R. Crespo-Otero, B. Demoulin, P. O. Dral, G. Granucci, F. Kossoski, H. Lischka, B. Mennucci, S. Mukherjee, M. Pederzoli, M. Persico, M. Pinheiro Jr, J. Pittner, F. Plasser, E. Sangiogo Gil and L. Stojanovic, *Journal of Chemical Theory and Computation*, 2022, **18**, 6851-6865.